NEURAL REGENERATION RESEARCH
December 2014, Volume 9, Issue 24
www.nrronline.org

A novel artificial nerve graft for repairing long-distance sciatic nerve defects: a self-assembling peptide nanofiber scaffold-containing poly(lactic-co-glycolic acid) conduit

Xianghai Wang[1], Mengjie Pan[1], Jinkun Wen[1], Yinjuan Tang[2], Audra D. Hamilton[3], Yuanyuan Li[1], Changhui Qian[1], Zhongying Liu[1], Wutian Wu[4, 5], Jiasong Guo[1, 6, 7]

1 Department of Histology and Embryology, Southern Medical University, Guangzhou, Guangdong Province, China
2 Department of Histology and Embryology, Xiangnan University, Chenzhou, Hunan Province, China
3 Department of Neurology, Vanderbilt University, Nashville, TN, USA
4 Department of Anatomy, Li Ka Shing Faculty of Medicine, The University of Hong Kong, Pokfulam, Hong Kong Special Administrative Region, China
5 GHM Institute of CNS Regeneration, Jinan University, Guangzhou, Guangdong Province, China
6 Key Laboratory of Tissue Construction and Detection of Guangdong Province, Guangzhou, Guangdong Province, China
7 Institute of Bone Biology, Academy of Orthopedics, Guangzhou, Guangdong Province, China

Corresponding author:
Jiasong Guo, Department of Histology and Embryology, Southern Medical University, Guangzhou 510515, China, jiasongguo@aliyun.com.

doi:*10.4103/1673-5374.147944*
http:*//www.nrronline.org/*

Accepted: *2014-10-06*

Abstract

In this study, we developed a novel artificial nerve graft termed self-assembling peptide nanofiber scaffold (SAPNS)-containing poly(lactic-co-glycolic acid) (PLGA) conduit (SPC) and used it to bridge a 10-mm-long sciatic nerve defect in the rat. Retrograde tracing, behavioral testing and histomorphometric analyses showed that compared with the empty PLGA conduit implantation group, the SPC implantation group had a larger number of growing and extending axons, a markedly increased diameter of regenerated axons and a greater thickness of the myelin sheath in the conduit. Furthermore, there was an increase in the size of the neuromuscular junction and myofiber diameter in the target muscle. These findings suggest that the novel artificial SPC nerve graft can promote axonal regeneration and remyelination in the transected peripheral nerve and can be used for repairing peripheral nerve injury.

Key Words: *nerve regeneration; peripheral nerve defect; artificial nerve graft; poly(lactic-co-glycolic acid); self-assembling peptide; nanofiber scaffold; remyelination; axon; myelin; neuromuscular junction; NSFC grants; neural regeneration*

Funding: *This work was supported by a grant from the National Key Basic Research Program of China, No. 2014CB542202 and 2014CB542205; the National Natural Science Foundation of China, No. 30973095 & 81371354; a grant from Science and Technology Project of Guangzhou, in China, No. 12C32121609; the Natural Science Foundation of Guangdong Province of China, No. S2013010014697 to Guo JS and Hong Kong SCI Fund to Wu WT.*

Wang XH, Pan MJ, Wen JK, Tang YJ, Hamilton AD, Li YY, Qian CH, Liu ZY, Wu WT, Guo JS. A novel artificial nerve graft for repairing long-distance sciatic nerve defects: a self-assembling peptide nanofiber scaffold-containing poly(lactic-co-glycolic acid) conduit. Neural Regen Res. 2014;9(24):2132-2141.

Introduction

Peripheral nerve injury is one of the most common clinical diseases, affecting 2.8% of all trauma patients (Noble et al., 1998; Bellamkonda, 2006; Zochodne, 2012). Direct repair is limited to short-distance gaps where the disconnected nerve stumps can be sutured end-to-end (Jiang and Zhang, 2010). Extensive nerve gaps must be reconstructed with structures, creating a permissive environment for neural regeneration, and eventually for reestablishing nerve function (Kuffler, 2014). Current clinical treatments for nerve defects typically rely on donor tissues, including nerve grafts, vein grafts and arterial grafts (Barcelos et al., 2003; Whitlock et al., 2009; Sun et al., 2011). However, these methods are limited by multiple disadvantages, such as a shortage of graft material, additional surgery trauma that results in functional loss at the donor sites, and the size and structural differences between donor and recipient. A promising alternative to conventional grafting is the use of artificial nerve grafts. Ideal biomaterials for neural tissue engineering should meet critical requirements, including excellent biocompatibility, biodegradability and neural integrity (Pfister et al., 2011).

Self-assembling peptide nanofiber scaffolds (SAPNSs) are novel biomaterials that have recently been extensively used in tissue engineering. Compared with traditional biomaterials, nanofibers have advantages in topography and porosity, thus mimicking the naturally occurring extracellular matrix.

They also exhibit excellent biocompatibility, low immunogenicity, are endowed with properties that help to bridge the lesion cavity or gap, and serve as an effective delivery system for graft cells or therapeutic drugs (Holmes, 2002; Guo et al., 2007). Using models of traumatic brain injury and spinal cord injury, we previously demonstrated that SAPNSs effectively facilitate central nervous system repair when administrated into the lesion cavities solely or in combination with cells/chemicals (Guo et al., 2007, 2009). Because the SAPNS is a gel-like soft material, it is difficult to use it to construct artificial peripheral nerve grafts, which are usually in the form of nerve tubes or conduits. In our previous report, we enhanced the SAPNS with an aorta canal segment serving as a conduit sheath to bridge a 10-mm nerve defect. By virtue of the multiple unique properties of the SAPNS conduit, peripheral nerve regeneration, motoneuronal protection, axonal remyelination, distal target reinnervation and locomotor functional recovery were significantly improved after 16 weeks compared with the group treated with the saline-filled empty conduit (Zhan et al., 2013).

Because the arterial conduit retains the limitations of natural grafts, in the present study, we developed a novel artificial nerve graft made of an outer porous poly(lactic-co-glycolic acid) (PLGA) conduit and an internal SAPNS. We named this graft SAPNS-containing PLGA conduit (SPC). All components of this nerve graft are synthesized biomaterials and are not restricted by the limitations of donor graft tissue. After transection, surgery was performed on the sciatic nerve of the rat, the SPC was transplanted to bridge the 10-mm gap of the transected nerve. Syngeneic peripheral nerves (PN) or empty PLGA conduits (EPC) were grafted as positive or negative controls, respectively. Using behavioral testing, retrograde tracing and histomorphometric analysis, we investigated the effectiveness of this novel artificial nerve graft for the repair of peripheral nerve injury.

Materials and Methods

Preparation of the SAPNS-containing PLGA conduit

PLGA was formed into a porous membrane with a thickness of 100 μm as previously described, with minor modifications (Sulong et al., 2014). Briefly, a 5% solution of 85:15 PLA:PGA, dissolved in dichloromethane, was control-poured into Teflon-coated horizontal molds. After evaporation of the solvent in a fume hood for 48 hours, the PLGA membrane was generated. A piece of PLGA membrane was wrapped onto a stainless rod with a diameter of 1.2 mm, and the ends of the membrane were then sealed with acetone. Thereafter, the rod was removed carefully and the remaining hollow cylindrical conduit of the PLGA was cut to 12 mm in length. The prepared PLGA conduits were sterilized and stored in 70% alcohol for further use.

After rinsing three times in DMEM culture medium (Invitrogen, Life Technologies, Carlsbad, CA, USA), the PLGA conduit was used to construct the SAPNS-containing conduit. 1% SAPNS solution consisting of RADA16-I peptide (BD Biosciences, Cambridge, MA, USA) was carefully filled into the full length of the conduit using a Hamilton microsyringe. Next, the conduit was immersed in DMEM medium for 30 minutes to trigger self-assembly of SAPNS for gelling, after which it was ready for transplantation (**Figure 1A, B**). For empty PLGA conduit transplantation, the conduit was rinsed with DMEM medium three times before application.

Animals and experimental groups

Fifty-four adult Sprague-Dawley (SD) female rats, weighing 200–250 g, were purchased from the Laboratory Animal Center of Southern Medical University, China, and were included in the study. Among these, 48 rats were used to prepare the model of sciatic nerve injury, and were randomly divided into four groups: (1) syngeneic peripheral nerve graft (PN; $n = 12$); (2) SAPNS-containing PLGA conduit (SPC; $n = 12$); (3) empty PLGA conduit (EPC; $n = 12$); and (4) non-graft control (NG; $n = 12$). The remaining six rats without sciatic nerve injury were used as a naive control.

Surgical procedures

The rats were anesthetized by intraperitoneal injection of 1% pentobarbital sodium, 3.5 mL/kg body weight. After routine skin preparation and disinfection, the right sciatic nerve was exposed and a transection was performed at the middle portion of the nerve trunk to prepare a 10-mm nerve defect. The SPC or EPC, with a length of 12 mm, was used to bridge the gap. The proximal and distal nerve stumps were inserted into the conduit to a distance of 1 mm and secured with 11-0 suture (Ethicon) (**Figure 1C**). For the positive control, a 10-mm segment of syngeneic fresh sciatic nerve obtained from donor rats was used to bridge the gap (PN group). In the NG group, the sciatic nerve with the 10-mm gap was left without any graft to serve as a negative control. Antibiotics and analgesic reagents were routinely administrated for postoperative health care. Guidelines for animal care and use of Southern Medical University, China were strictly followed. The animals were allowed access to food and water *ad libitum* throughout the study.

Behavioral testing

Recovery of hindlimb motor function was assessed with a modified sciatic function index (SFI) at 15 weeks post-treatment as in a previous report (de Medinaceli et al., 1982). Briefly, the palms of the forelimbs and hindlimbs were colored with different nontoxic dyes. The animals were then trained to walk on a paper-covered narrow runway (1 m long, 7 cm wide and 8 cm high). To perform the assessments, each rat was tested three times, and the first and last 15 cm of the print were excluded. Some seriously injured hindlimbs could not leave adequate footprints on the paper-covered runway. We classified the footprints into three patterns, and the percentage of each pattern was calculated as follows: (1) dragged, indicating no footprint left on the paper due to the injured hindlimb not attaching to the paper or supported with the dorsum pedis; (2) heel supported, indicating that only the heel of the foot left a print on the paper; (3) palm supported, indicating an adequate footprint, including the heel and toes. Six adequate footprints for each rat were se-

lected to measure (i) the angle subtended by the stride line and the line connecting the third toe to the center of the paw pad (rotation angle of the injured foot; RAF), and (ii) the distance between the center pads of the injured hindlimb and ipsilateral forelimb (distance between the injured hindlimb and forelimb; DHF).

Retrograde tracing

To visualize motor neurons in the ventral horn of the spinal cord whose axons had regenerated and passed through the implants, Fluoro-Gold was used for retrograde tracing as previously reported (Zele et al., 2010). Fifteen weeks after transplantation surgery, 2 μL of 1% Fluoro-Gold (Sigma, St. Louis, MO, USA) was microinjected at the site on the nerve trunk 5 mm distal to the nerve-implant suture site using a Hamilton syringe with a 30-gauge needle. The injection needle was slowly withdrawn after 2 minutes. Animals were allowed to survive for another 7 days for tracer transportation before they were sacrificed.

Tissue collection

Seven days after retrograde tracing (16 weeks post-transplantation), animals were euthanized with an overdose of anesthesia and transcardially perfused with 4% paraformaldehyde in 0.1 mol/L phosphate buffer (pH 7.4). Bilateral gastrocnemius muscles were explanted immediately, and the wet muscle weight was measured on a laboratory scale (Mettler Toledo, Greifensee, Switzerland). The weight ratio of the injured side to the intact side was calculated and used as the recovery index of the gastrocnemius muscle. Then, the muscles were post-fixed with 4% paraformaldehyde for histomorphometry. The sciatic nerve segments containing the conduit implants and the 5th lumbar (L_5) segment of the spinal cord were also harvested after perfusion. Three nerve samples for each group were post-fixed with 2.5% glutaraldehyde/2% paraformaldehyde for transmission electron microscopy. The remaining samples were post-fixed with 4% paraformaldehyde for cryosectioning and immunofluorescence staining.

Transmission electron microscopy

From the selected nerve samples, a 1-mm-long segment from the middle of the graft, or the corresponding site of naive control sciatic nerve, was dissected for transmission electron microscopy as previously described (Zhan et al., 2013). After fixation with 2.5% glutaraldehyde/2% paraformaldehyde for 24 hours, the samples were post-fixed in 1% OsO_4 for 2 hours at 4 °C and dehydrated in a graded acetone series. The samples were then embedded with Spurr's resin (Sigma) for ultrathin transverse sectioning (70 nm) and counterstaining with 2% uranyl acetate and lead citrate. The stained ultrathin sections were observed with a transmission electron microscope (H-7500, Hitachi). Six random non-overlapping images of each sample were captured for the following assessments: (1) myelin thickness; (2) axonal diameter; (3) G-ratio of the myelinated nerve fiber, which was determined by dividing axon diameter by the diameter of the whole myelinated fiber; and (4) myelinated axon ratio, which was calculated by counting the number of myelinated axons divided by the number of total axons. The measurements were obtained using Image-Pro Plus software (Media Cybernetics, Bethesda, MD, USA).

Immunofluorescence staining

The samples designated for immunofluorescence staining were embedded in optimal cutting temperature compound (Leica) after post-fixation in 4% paraformaldehyde for 24 hours, then immersed in 30% sucrose (w/v) until the samples sank in the sucrose solution. Three nerves from each transplantation group (PN, SPC and EPC groups) were cryosectioned longitudinally to obtain sections including the whole graft and 0.5 mm of the host nerve trunk on both sides. The remaining implants were transversally cryosectioned commencing 1 mm proximal or distal to the sutured site until the midpoint of the implant. All sections were cut to 10 μm thickness, mounted onto poly-L-lysine coated slides, and then kept at −20°C until use.

Every tenth section of each sample was double immunostained with NF200/myelin basic protein (MBP) to detect the axon and myelin. Selected sections were washed with PBS three times (5 minutes each) and blocked with 5% gelatin from cold water fish skin (Sigma) and 0.3% Triton X-100 in 0.1 mol/L PBS for 1 hour at room temperature. Subsequently, sections were incubated with polyclonal rabbit anti-NF200 (1:500; Sigma) and monoclonal mouse anti-MBP (1:500; Santa Cruz Biotechnology, Santa Cruz, CA, USA) overnight at 4°C. The samples were then incubated with Alexa 568-conjugated goat anti-rabbit and Alexa 488-conjugated goat anti-mouse secondary antibodies (1:400; Molecular Probes) for 2 hours at room temperature. The slides were coverslipped with mounting medium containing 4′,6-diamidino-2-phenylindole (DAPI; Dako) to stain nuclei. Digital images were captured with a fluorescence microscope (Leica, DM4000B).

Alkaline phosphatase histochemistry

Vascularization in the graft was assessed in randomly selected longitudinal sections of each sample by alkaline phosphatase histochemistry as previously described (Guo et al., 2007).

Quantification of surviving and regenerating neurons

The 5th lumbar (L_5) segment of the spinal cord was cryosectioned transversally at 10 μm thickness and then stained with the fluorescent Nissl staining kit (1:500; Sigma) following the vendor's instructions. Every eighth section of each sample was selected to count surviving and regenerating motor neurons in the spinal cord ventral horn. The motor neurons were identified by their large size, location and dark Nissl staining (Watson et al., 2001). The survival rate of the motor neurons was calculated as the ratio of the number of neurons in the injured side divided by the number of neurons in the intact side. The regeneration rate was calculated as the number of Fluoro-Gold-labeled neurons divided by the number of Nissl-stained neurons in the injured side.

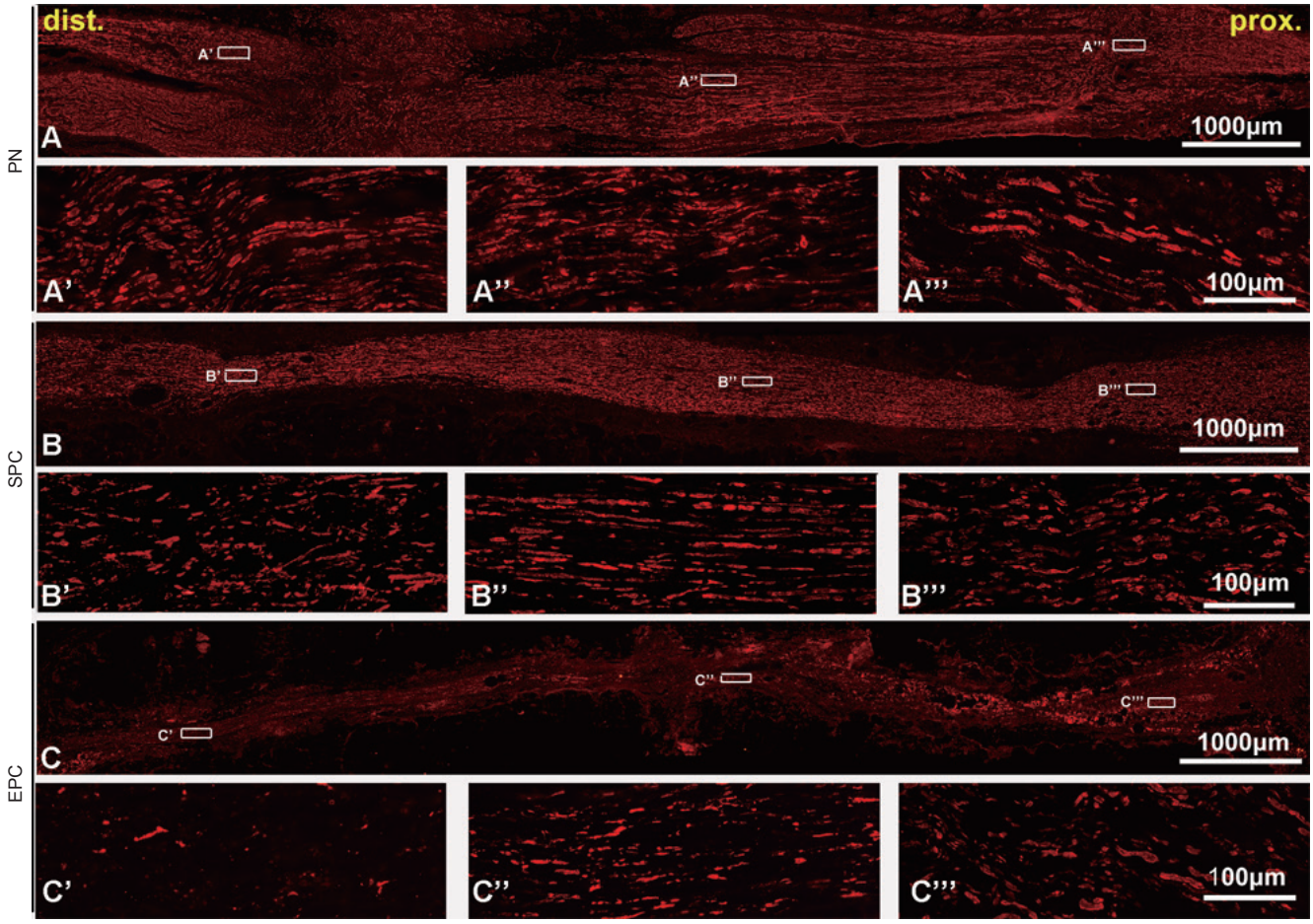

Figure 2 Longitudinal sciatic nerve sections of conduit implants immunostained with NF200 showing regenerated axons in the grafts.
Longitudinal sections, immunostained with the axonal marker NF200 (red), showing robust axonal regeneration into the PN (A–A''') and SPC (B–B''') grafts, which was much greater than in the EPC graft C–C'''. A'–A''', B'–B''' and C'–C''' are higher-power magnifications of the corresponding boxed areas in A, B and C, respectively. PN: Syngeneic peripheral nerve; SPC: self-assembling peptide nanofiber scaffold-containing poly(lactic-co-glycolic acid) conduit; EPC: empty poly(lactic-co-glycolic acid) conduit; dist: distal; prox: proximal.

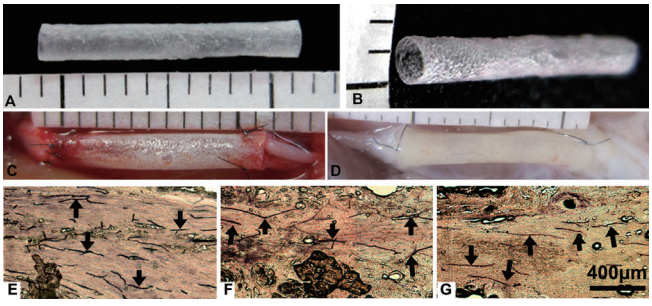

Figure 1 A sample of artificial nerve conduit used to bridge the sciatic nerve defect.
A conduit made of porous poly(lactic-co-glycolic acid) membrane, 12 mm in length and 1.5 mm in diameter (A, B). This conduit was filled with self-assembling peptide nanofiber scaffold to fabricate an artificial nerve graft, which was then used to bridge the 1-mm gap of a transected sciatic nerve. Both proximal and distal nerve stumps were inserted 1 mm into the conduit, and the connections were secured with 11-0 suture (C). At 16 weeks after transplantation, the implant had integrated properly with the host nerve, and there was no significant scarring (D). (E–G) Alkaline phosphatase histochemistry showing angioregeneration (arrows) in the proximal (E), middle (F) and distal (G) part of a sample of self-assembling peptide nanofiber scaffold-containing poly(lactic-co-glycolic acid) conduit. Scale bar for E–G is 400 μm.

Histomorphometry of the gastrocnemius muscle and neuromuscular junction

The mid-belly of the gastrocnemius muscle was trimmed for cryosectioning after post-fixation with 4% paraformaldehyde. Two sets of sections were prepared from each animal; one set was transversally sectioned for routine hematoxylin staining to count the number of muscular fibers. The second set was longitudinally sectioned for neuromuscular junction staining with α-bungarotoxin (α-BTX; 1:500; Sigma) as previously described (Anderson et al., 1984). The area of the junction was calculated. All quantifications were done in six random non-overlapping fields of every eighth section of each animal using Image-Pro Plus software.

Statistical analysis

All values are presented as the mean ± SD. SPSS 13.0 software for Windows (SPSS, Chicago, IL, USA) was used for statistical analysis. One-way analysis of variance followed by Bonferroni *post hoc* comparison was used to analyze intergroup differences. $P < 0.05$ was considered a statistically significant difference.

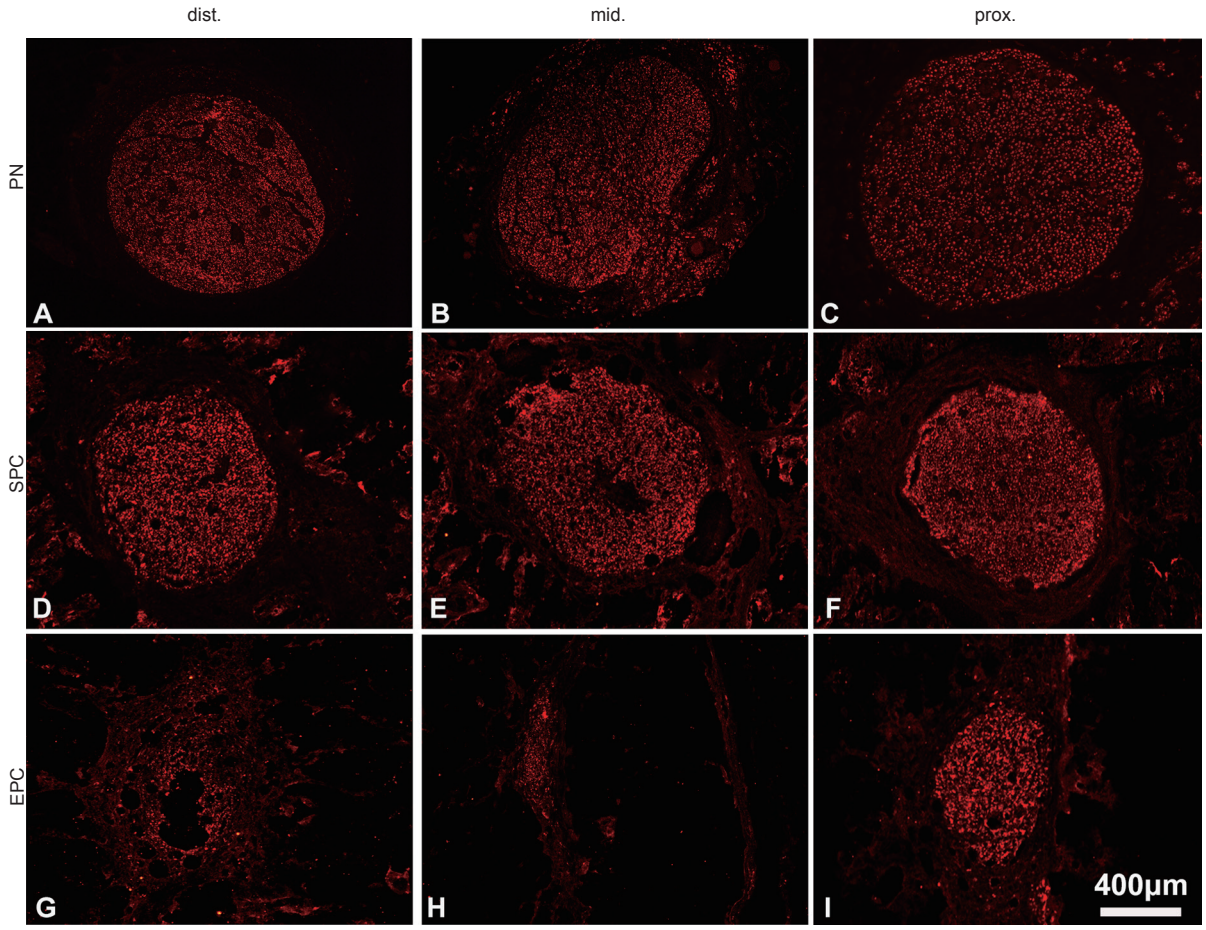

Figure 3 Transverse sections of sciatic nerve conduit implants immunostained with NF200 showing regenerated axons in the grafts.
Transverse sections immunostained with the axonal marker NF200 (red) showing regenerated axons in the proximal, middle and distal segments of PN (A–C), SPC (D–F) and EPC (G–I) grafts. Of note, the overall axon distribution in the SPC was similar to that in the PN implant. In contrast, only the proximal part of the EPC was moderately filled with axons, and fewer axons were present in the middle and distal parts of the EPC. PN: Syngeneic peripheral nerve; SPC: self-assembling peptide nanofiber scaffold-containing poly(lactic-co-glycolic acid) conduit; EPC: empty poly(lactic-co-glycolic acid) conduit; dist: distal; mid: middle; prox: proximal.

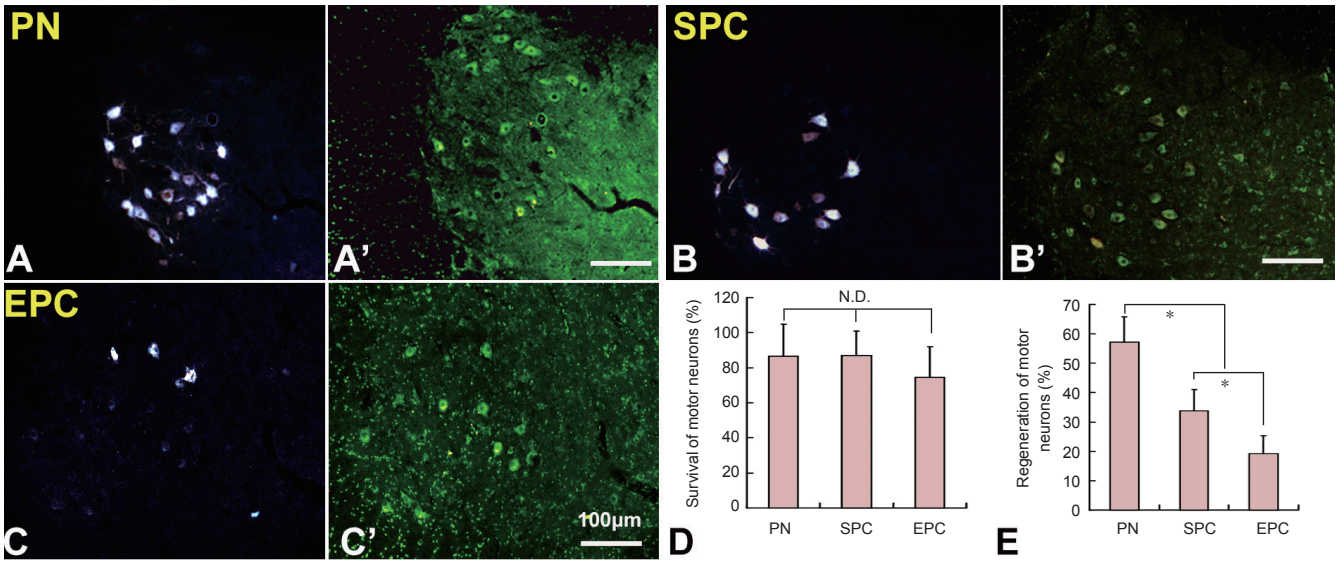

Figure 5 Survival and regeneration of injured motor neurons in the spinal cord.
Fluoro-Gold retrograde labeling of regenerated spinal motor neurons (yellow) in the PN (A), SPC (B) and EPC (C) groups. A', B' and C' are representative images of Nissl staining (green) showing the surviving neurons in the fields in A, B and C, respectively. D, E show the quantification of survival (D) and regeneration (E) of the spinal motoneurons. The data are expressed as the mean ± SD. One-way analysis of variance followed by Bonferroni *post hoc* comparison was used to analyze intergroup differences. $*P < 0$ .05, $^{N.D.}P > 0.05$. PN: Syngeneic peripheral nerve; SPC: self-assembling peptide nanofiber scaffold-containing poly(lactic-co-glycolic acid) conduit; EPC: empty poly(lactic-co-glycolic acid) conduit.

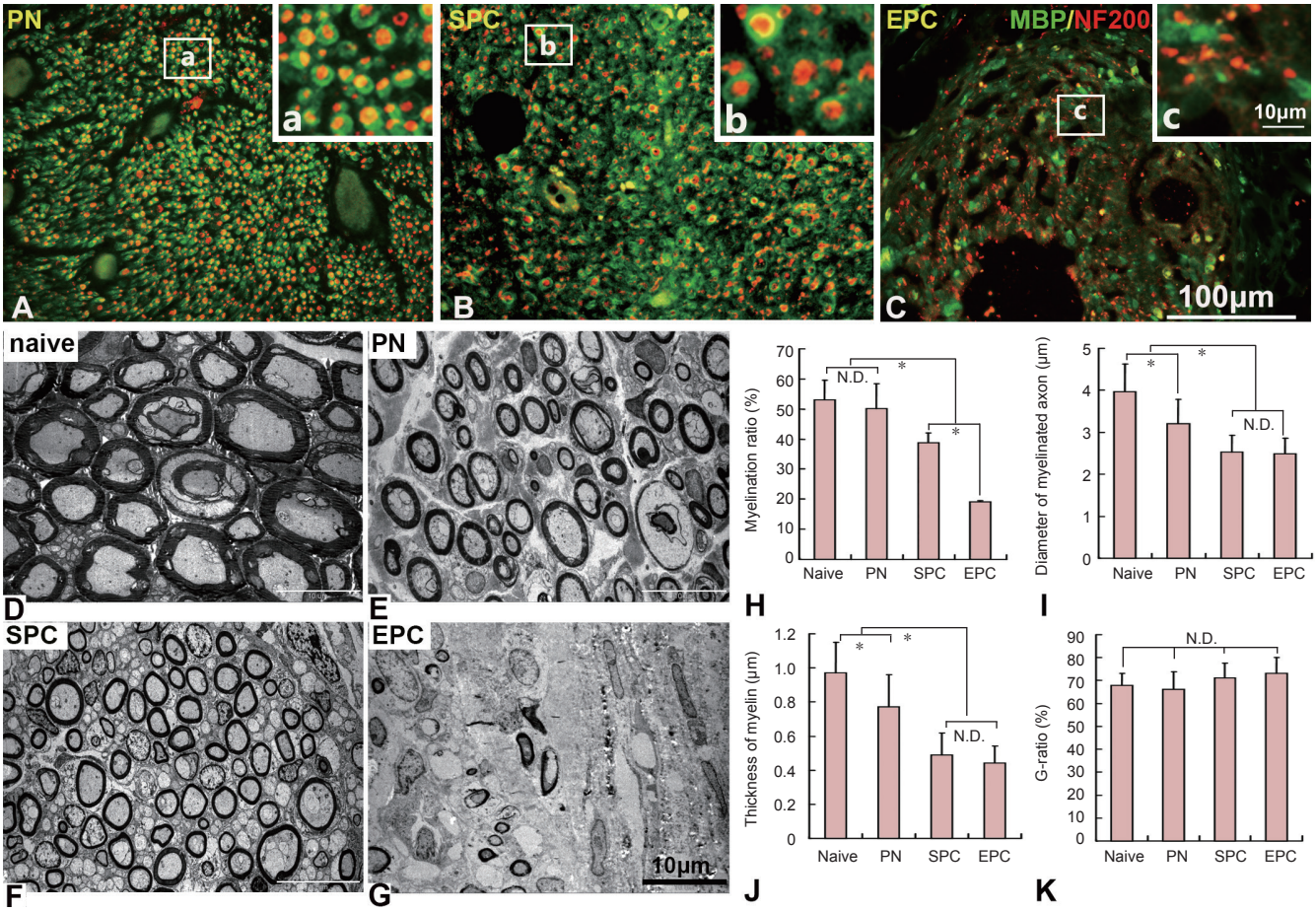

Figure 4 Immunofluorescence staining and transmission electron microscopy (TEM) showing the remyelination of regenerated axons in the nerve conduits.

(A–C) MBP (green) and NF200 (red) double immunostaining showing significant remyelination of regenerated axons in the middle part of the PN (A) and SPC (B) grafts, but limited remyelination in the EPC graft (C). a–c are magnified images of the boxed areas in A–C. (D–G) TEM showing the presence of typical remyelinated fibers in all implant types (E, PN group; F, SPC group; G, EPC group), although the diameter of the fibers and the thickness of the myelin were less than in the naive nerve (D). (H–K) Quantification showing the remyelination rate of axons (H), axon diameter (I), myelin thickness (J) and G-ratio (K) of the myelinated fibers in the various groups. The data are expressed as the mean ± SD. One-way analysis of variance followed by Bonferroni *post hoc* comparison was used to analyze intergroup differences. $*P < 0.05$, $^{N.D}P > 0.05$. PN: Syngeneic peripheral nerve; SPC: self-assembling peptide nanofiber scaffold-containing poly(lactic-co-glycolic acid) conduit; EPC: empty poly(lactic-co-glycolic acid) conduit.

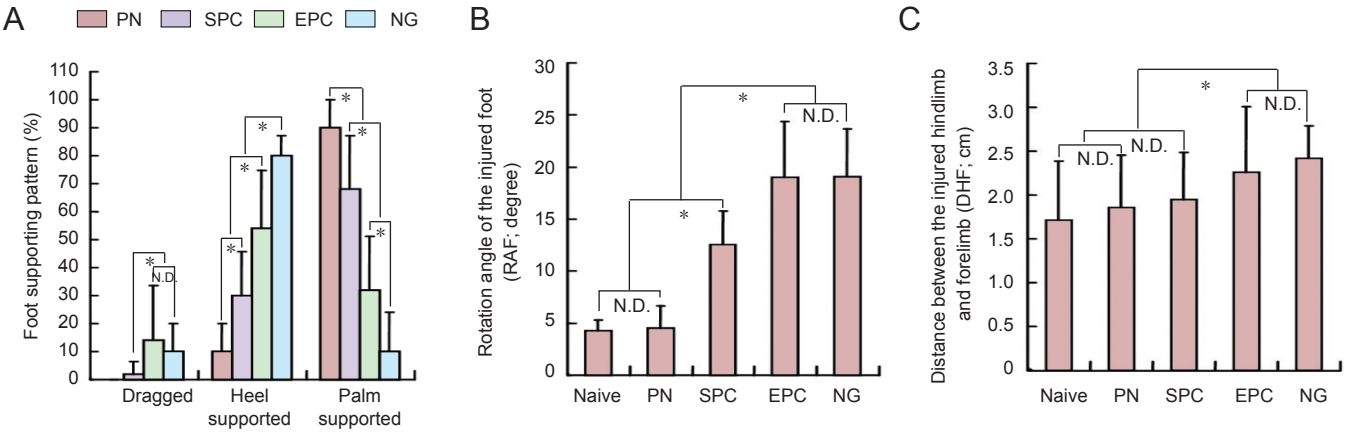

Figure 8 Functional recovery of the injured hindlimb in rats with sciatic nerve transection following nerve conduit implantation.

The motor functional recovery of the injured hindlimb was quantified with footprint testing. Bar graphs showing the percentage of foot supported pattern (A), rotation angle of the injured foot (RAF; B), and the distance between the center pads of the injured hindlimb and ipsilateral forelimb (distance between the injured hindlimb and forelimb; DHF) (C) in each group. The data are expressed as the mean ± SD. One-way analysis of variance followed by Bonferroni *post hoc* comparison was used to analyze intergroup differences. $*P < 0.05$, $^{N.D}P > 0.05$. PN: Syngeneic peripheral nerve; SPC: self-assembling peptide nanofiber scaffold-containing poly(lactic-co-glycolic acid) conduit; EPC: empty poly(lactic-co-glycolic acid) conduit; NG: non-graft control.

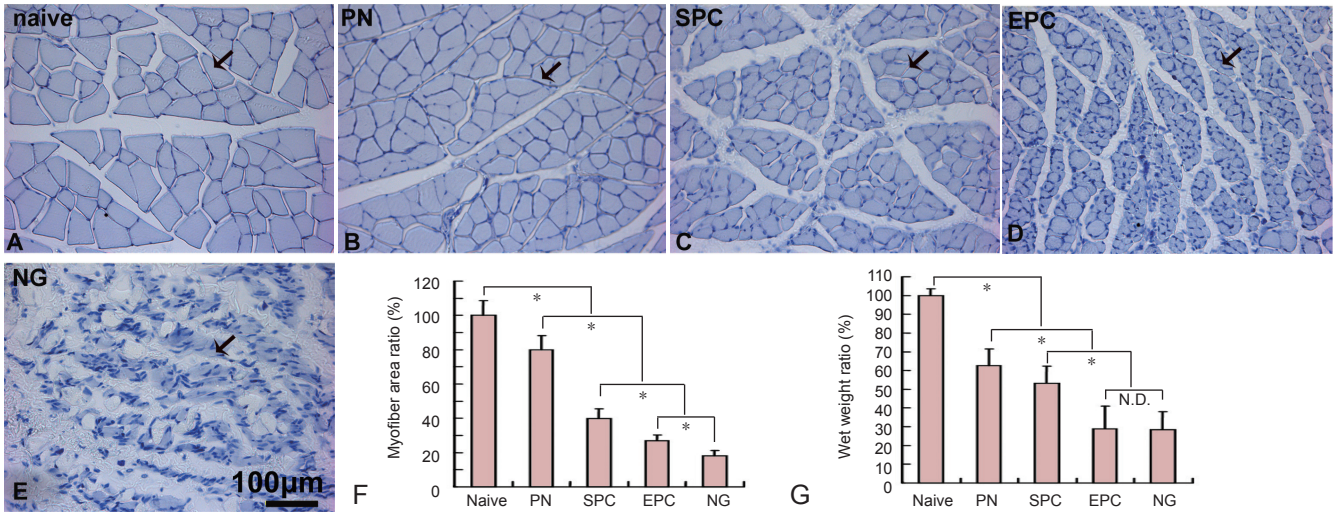

Figure 6 The morphology and wet weight of the gastrocnemius muscle in rats with sciatic nerve transection following nerve conduit implantation.
Hematoxylin-stained sections of the naive (A), PN (B), SPC (C), EPC (D) and NG (E) groups showing the morphology of the myofibers (arrows). Serious steatosis and myoatrophy appeared in the NG group, while steatosis and myoatrophy were ameliorated with the implants. The level of myoatrophy was assessed by quantification of myofiber ratio (F) and wet weight ratio (G). The data are expressed as the mean ± SD. One-way analysis of variance followed by Bonferroni *post hoc* comparison was used to analyze intergroup differences. $*P < 0.05$, $^{N.D.}P > 0.05$. PN: Syngeneic peripheral nerve; SPC: self-assembling peptide nanofiber scaffold-containing poly(lactic-co-glycolic acid) conduit; EPC: empty poly(lactic-co-glycolic acid) conduit; NG: non-graft control.

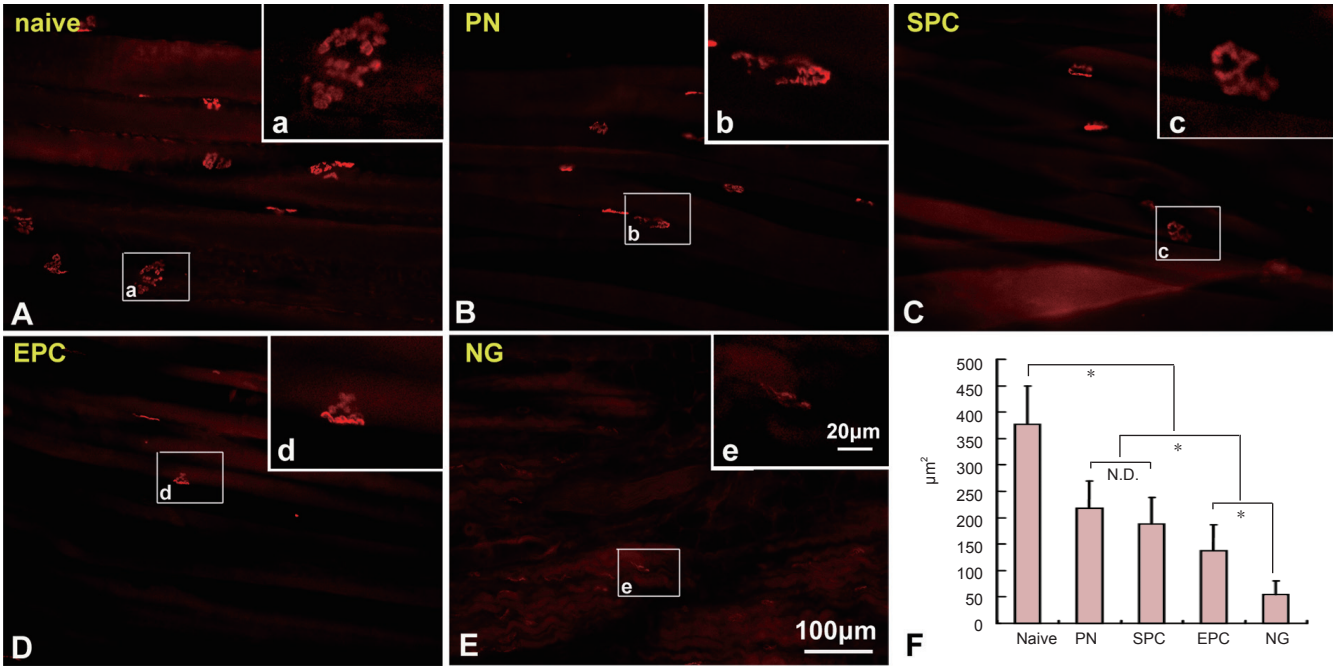

Figure 7 Histomorphometry of the neuromuscular junction in the gastrocnemius muscle of rats with sciatic nerve transection following nerve conduit implantation.
α-BTX-stained longitudinal gastrocnemius muscle sections showing neuromuscular junctions in the naive group (A), PN group (B), SPC group (C), EPC group (D) and NG group (E). a–e are magnified images of the boxed areas in A–E. In the injured groups (B–E), the junctions were reduced in size to varying degrees, and were all significantly smaller than in the naive group (A). (F) Quantification showing the size of the neuromuscular junctions in each group. The data are expressed as the mean ± SD. One-way analysis of variance followed by Bonferroni *post hoc* comparison was used to analyze intergroup differences. $*P < 0.05$, $^{N.D.}P > 0.05$. PN: Syngeneic peripheral nerve; SPC: self-assembling peptide nanofiber scaffold-containing poly(lactic-co-glycolic acid) conduit; EPC: empty poly(lactic-co-glycolic acid) conduit; NG: non-graft control.

Results

Axonal regeneration in the conduit

At 16 weeks after transplantation, both SPC and EPC grafts had integrated properly with the host nerve, and there was no significant scarring (**Figure 1D**). Moreover, angioregeneration was found in SPC grafts from proximal to distal areas (**Figure 1E–G**). On longitudinal sections, robustly NF200-labeled axons were visible in the SPC implant (**Figure 2B–**

B'"). Notably, axons grew with a linear profile. On transverse sections, the axons almost fully filled the entire conduit (**Figure 3D–F**). The overall axon distribution in the SPC grafts was similar to that in the PN grafts (**Figures 2A–A'", 3A–C**). In contrast, only the proximal part of the EPC implant was moderately filled with axons; fewer axons were present in the middle and distal parts of the EPC implant (**Figures 2C–C'", 3G–I**).

Remyelination of regenerated axons

Double staining with NF200 and MBP antibodies showed that many NF200-positive axons in the implant were wrapped with MBP-positive myelin (**Figure 4A–C**). To better evaluate regeneration efficiency and remyelination, we examined ultrathin transverse sections of the middle segment of the implants with transmission electron microscopy. The regenerated axons and myelin in the PN and SPC groups were smaller than in the naive sciatic nerve, but the regenerated axons almost completely filled the implants, and many of these were myelinated (**Figure 4D–F**). In the EPC grafts, the regenerated axons were scattered mainly around the edges of the conduit (**Figure 4G**). Quantification demonstrated that the remyelination rate of axons was significantly higher in the SPC group than in the EPC group ($P < 0.05$), but was lower than in the naive and PN groups ($P < 0.05$) (**Figure 4H**). There was no statistically significant difference in axon diameter or myelin thickness between the SPC and EPC groups. However, axon diameter and myelin thickness in the SPC and EPC groups were significantly less than in the naive and PN groups ($P < 0.05$) (**Figure 4I, J**). Additionally, the G-ratio of myelinated fibers was lowest in the naive group, and highest in the EPC group; however, no statistically significant difference was detected among the groups ($P > 0.05$) (**Figure 4K**).

Survival and regeneration of damaged neurons

As motoneurons in the lumbar spinal cord extend their axons into the sciatic nerve, they were injured during the sciatic nerve transection, which could result in cell death. Unexpectedly, compared with the intact side, almost 86% of neurons survived in the PN and SPC groups. The survival rate was decreased to 74.2% in the EPC group, but there was no significant difference among the PN, SPC and EPC groups ($P > 0.05$) (**Figure 5A'–C', D**). Fluoro-Gold retrograde labeling demonstrated that 57.1 ± 8.6%, 33.8 ± 7.3% and 19.1 ± 6.1% of motoneurons in the ipsilateral ventral horn had regenerated axons in the PN, SPC and EPC groups, respectively (**Figure 5A–C, E**). There were statistically significant differences among the groups ($P < 0.05$).

Gastrocnemius muscle wet weight and muscle morphology

At 16 weeks after sciatic nerve transection, the gastrocnemius muscle lost weight dramatically and showed serious steatosis and atrophy in the NG group, which did not receive an implant, and the targeted gastrocnemius muscle suffered from chronic denervation. In contrast, steatosis and myoatrophy were ameliorated by the implants (**Figure 6A–E**). Quantification showed that the ratio of the myofiber transverse area in the injured to the intact side was 79.8 ± 8.5%, 39.9 ± 5.5%, 26.9 ± 3.4% and 18.1 ± 3.1% in the PN, SPC, EPC and NG groups, respectively. Differences between these groups were statistically significant ($P < 0.05$) (**Figure 6F**). Correspondingly, the whole gastrocnemius muscle wet weight ratio of the injured to the intact side was 62.45 ± 9.10%, 53.16 ± 9.18%, 28.97 ± 11.98% and 28.38 ± 9.68% in the PN, SPC, EPC and NG groups, respectively. Differences between these groups were statistically significant ($P < 0.05$), with the exception of the EPC group *vs.* NG group ($P > 0.05$) (**Figure 6G**).

Assessment of the neuromuscular junction

Using α-BTX-stained longitudinal gastrocnemius muscle sections, the neuromuscular junction was clearly visible. In the nerve injury groups, the junctions were reduced in size to varying degrees and were significantly smaller than in the naive group ($P < 0.05$). The NG group had the smallest junction, followed by the EPC and SPC groups. The neuromuscular junction was largest in the PN group. There were significant differences among the groups, with the exception of SPC *vs.* PN (**Figure 7**).

Functional recovery of the injured hindlimb

When the locomotor function of the injured hindlimb was assessed by footprint testing to assess SFI, we found that almost 90% of footprints left by injured hindlimbs in the NG group displayed an impairment of foot positioning on the paper-covered runway. 10.2% of ipsilateral footprints were classified as "dragged" and 79.3% were categorized as "heel supported" (having only a heel print). Only 10.5% of footprints included heel and toes (palm supported). Quantification data showed that the percentage of palm-supported steps was higher among the various implant groups, increasing in the following order: EPC group, SPC group, PN group. There were significant differences among the groups ($P < 0.05$) (**Figure 8A**). Six palm-supported footprints for each rat were selected to measure the rotation angle of the injured foot (RAF) and the distance between the center pads of the injured hindlimb and ipsilateral forelimb (DHF). Because of the motor function impairment, these values were increased after injury. The RAF and DHF values were slightly increased in the PN group compared with the naive group ($P > 0.05$), but significantly increased in the NG and EPC groups (there was no statistically significant difference between the NG and EPC groups, $P > 0.05$). RAF in the SPC group was significantly lower than in the NG and EPC groups ($P < 0.05$), but was still significantly higher than in the naive and PN groups ($P < 0.05$) (**Figure 8B**). The DHF in the SPC group was significantly lower than in the NG group ($P < 0.05$), but there was no significant difference from the other groups ($P > 0.05$). The trend was similar to the RAF values (**Figure 8C**).

Discussion

A variety of artificial nerve grafts have been evaluated for peripheral nerve repair. Tissue-engineered artificial nerve grafts include biomaterial scaffolds, seed cells and biological-

ly active molecules (Angius et al., 2012). In these grafts, the biomaterial is most critical. The SAPNS used in the present study is made of a novel self-assembling peptide, RADA16-I (AcN-RADARADARADARADA-CNH2), which is composed of alternating positive and negative L-amino acid arrangements (Zhang et al., 1993; Cormier et al., 2013). It can be spontaneously self-assembled into nanofibers in the presence of physiological solutions or body fluids (Zhang et al., 2005). The nanofibers form a hydrogel scaffold with greater than 99% water content. Several studies have revealed that the nanoscale peptide scaffold presents a true three-dimensional environment similar to the natural extracellular matrix (Ellis-Behnke et al., 2006; Zhang, 2008; Alluin et al., 2009; Volpato et al., 2013). Therefore, it is able to support the adhesion, proliferation and differentiation of various cells. Our previous study showed that an SAPNS-containing arterial conduit could significantly promote neural regeneration in the damaged sciatic nerve (Zhan et al., 2013). This demonstrates that SAPNS has potential for peripheral nerve repair. However, the nerve conduit is critical for regeneration. Therefore, in the present study, we evaluated an alternative material for forming the conduit.

PLGA is a synthetic polymer that has exhibited great promise for applications in the field of tissue engineering because of its biocompatibility and biodegradability (Cohen et al., 1991; Gref et al., 1994; Jain, 2000; Li et al., 2002). We developed a conduit with a porous PLGA membrane. Optimal membrane porosity is crucial for the movement and exchange of nutrients between the tissues inside the conduit and the surroundings. This feature is very important in the early stage of transplantation because blood vessels have not yet regenerated in the graft. Another advantage of the artificial PLGA conduit is that the diameter and length of the conduit can be adjusted to the size and gap distance of the nerve defect.

The present data revealed that the SPC graft can effectively promote peripheral axonal regeneration over a 10-mm gap. Longitudinal sections showed that NF200-positive regenerated axons displayed well-ordered arrangements in the graft, and passed through the defect and connected both stumps. Transverse sections showed that the regenerated axons almost fully filled the implants in the PN and SPC groups. However, in the EPC grafts, the regenerated axons were scattered around the edge of the conduit. Furthermore, spinal motor axonal regeneration was confirmed by retrograde labeling with Fluoro-Gold tracer.

Myelination level can affect the conduction velocity of regenerated nerve fibers. In double-immunostained sections, many NF200-positive regenerated axons in the implants were wrapped with MBP-positive myelin. When we assessed the ultrathin transverse sections with transmission electron microscopy, quantification demonstrated that the remyelination rate of axons was significantly higher in the SPC group than in the EPC group, but lower than in the naive and PN groups. Additionally, the G-ratio of myelinated fibers was lowest in the naive group, followed by the PN group and the SPC group. It was highest in the EPC group, and no significant difference was detected among the groups. Collectively, these data indicate that SPC grafts contribute to an increase in the number of regenerated axons and remyelination rate.

Denervation and loss of function in target muscle is a serious consequence of peripheral nerve injury. The gastrocnemius muscle was used as a representative target muscle of the sciatic nerve in this study. At 16 weeks after sciatic nerve injury, the wet weight ratio showed a dramatic decrease in the NG group, which did not have any treatment after surgery. Morphological observations demonstrated serious steatosis, myoatrophy and neuromuscular junction degeneration in the NG group. In contrast, steatosis and myoatrophy were ameliorated with the implants. We quantified the wet weight ratio and the myofiber transverse area ratio of the injured to the intact side, as well as the area of the neuromuscular junction, to evaluate myoatrophy. These values increased in the following order: NG, EPC, SPC, PN and naive groups. These findings are consistent with the locomotor function assessments. Overall, these findings indicate that the SPC, PN and EPC grafts promote sciatic nerve regeneration, leading to reinnervation of target muscle to different degrees.

In the present study, we used syngeneic nerve graft (*i.e.*, the PN graft) as a positive control, because it has similar outcomes to nerve autograft in animal models (Ray and Mackinnon, 2010). The SPC graft efficiently reconstructed the nerve and restored nerve continuity and function, and the overall outcomes were markedly better than those achieved with the EPC graft. However, the outcome of the SPC graft was not as good as that of the PN graft. Nonetheless, because the SAPNS in the artificial nerve graft is an ideal material for cell and drug delivery, the SPC graft might hold significant therapeutic potential for peripheral nerve repair. We expect that much better outcomes will be achieved once functional proteins, therapeutic macromolecules, bioactive motifs and seed cells are combined into the internal SAPNS structure of the SPC graft in the future.

Taken together, our findings show that the SPC nerve graft significantly improves axonal regeneration and remyelination, ameliorates hindlimb deficits, and reduces myoatrophy and neuromuscular junction degeneration in target muscle.

Author contributions: *Guo JS, Wu WT and Wang XH conceived and designed this study. Wang XH conducted the majority of the experiments. Pan MJ, Wen JK, Tang YJ, Qian CH, Liu ZY and Li YY contributed to data collection and analysis. Guo JS, Wang XH, Wu WT and Hamilton AD drafted the manuscript. All authors approved the final version of this paper.*
Conflicts of interest: *None declared.*

References

Alluin O, Wittmann C, Marqueste T, Chabas JF, Garcia S, Lavaut MN, Guinard D, Feron F, Decherchi P (2009) Functional recovery after peripheral nerve injury and implantation of a collagen guide. Biomaterials 30:363-373.

Anderson MJ, Klier FG, Tanguay KE (1984) Acetylcholine receptor aggregation parallels the deposition of a basal lamina proteoglycan during development of the neuromuscular junction. J Cell Biol 99:1769-1784.

Angius D, Wang H, Spinner RJ, Gutierrez-Cotto Y, Yaszemski MJ, Windebank AJ (2012) A systematic review of animal models used to study nerve regeneration in tissue-engineered scaffolds. Biomaterials 33:8034-8039.

Barcelos AS, Rodrigues AC, Silva MD, Padovani CR (2003) Inside-out vein graft and inside-out artery graft in rat sciatic nerve repair. Microsurgery 23:66-71.

Bellamkonda RV (2006) Peripheral nerve regeneration: an opinion on channels, scaffolds and anisotropy. Biomaterials 27:3515-3518.

Cohen S, Yoshioka T, Lucarelli M, Hwang LH, Langer R (1991) Controlled delivery systems for proteins based on poly(lactic/glycolic acid) microspheres. Pharm Res 8:713-720.

Cormier AR, Pang X, Zimmerman MI, Zhou HX, Paravastu AK (2013) Molecular structure of RADA16-I designer self-assembling peptide nanofibers. ACS Nano 7:7562-7572.

de Medinaceli L, Freed WJ, Wyatt RJ (1982) An index of the functional condition of rat sciatic nerve based on measurements made from walking tracks. Exp Neurol 77:634-643.

Ellis-Behnke RG, Liang YX, You SW, Tay DK, Zhang S, So KF, Schneider GE (2006) Nano neuro knitting: peptide nanofiber scaffold for brain repair and axon regeneration with functional return of vision. Proc Natl Acad Sci U S A 103:5054-5059.

Gref R, Minamitake Y, Peracchia MT, Trubetskoy V, Torchilin V, Langer R (1994) Biodegradable long-circulating polymeric nanospheres. Science 263:1600-1603.

Guo J, Su H, Zeng Y, Liang YX, Wong WM, Ellis-Behnke RG, So KF, Wu W (2007) Reknitting the injured spinal cord by self-assembling peptide nanofiber scaffold. Nanomedicine 3:311-321.

Guo J, Leung KK, Su H, Yuan Q, Wang L, Chu TH, Zhang W, Pu JK, Ng GK, Wong WM, Dai X, Wu W (2009) Self-assembling peptide nanofiber scaffold promotes the reconstruction of acutely injured brain. Nanomedicine 5:345-351.

Holmes TC (2002) Novel peptide-based biomaterial scaffolds for tissue engineering. Trends Biotechnol 20:16-21.

Jain RA (2000) The manufacturing techniques of various drug loaded biodegradable poly(lactide-co-glycolide) (PLGA) devices. Biomaterials 21:2475-2490.

Jiang B, Zhang P (2010) Advances in small gap sleeve bridging peripheral nerve injury. Artif Cells Blood Substit Immobil Biotechnol 38:1-4.

Kuffler DP (2014) An assessment of current techniques for inducing axon regeneration and neurological recovery following peripheral nerve trauma. Prog Neurobiol 116:1-12.

Li WJ, Laurencin CT, Caterson EJ, Tuan RS, Ko FK (2002) Electrospun nanofibrous structure: a novel scaffold for tissue engineering. J Biomed Mater Res 60:613-621.

Noble J, Munro CA, Prasad VS, Midha R (1998) Analysis of upper and lower extremity peripheral nerve injuries in a population of patients with multiple injuries. J Trauma 45:116-122.

Pfister BJ, Gordon T, Loverde JR, Kochar AS, Mackinnon SE, Cullen DK (2011) Biomedical engineering strategies for peripheral nerve repair: surgical applications, state of the art, and future challenges. Crit Rev Biomed Eng 39:81-124.

Ray WZ, Mackinnon SE (2010) Management of nerve gaps: autografts, allografts, nerve transfers, and end-to-side neurorrhaphy. Exp Neurol 223:77-85.

Sulong AF, Hassan NH, Hwei NM, Lokanathan Y, Naicker AS, Abdullah S, Yusof MR, Htwe O, Idrus RB, Haflah NH (2014) Collagen-coated polylactic-glycolic acid (PLGA) seeded with neural-differentiated human mesenchymal stem cells as a potential nerve conduit. Adv Clin Exp Med 23:353-362.

Sun F, Zhou K, Mi WJ, Qiu JH (2011) Combined use of decellularized allogeneic artery conduits with autologous transdifferentiated adipose-derived stem cells for facial nerve regeneration in rats. Biomaterials 32:8118-8128.

Volpato FZ, Fuhrmann T, Migliaresi C, Hutmacher DW, Dalton PD (2013) Using extracellular matrix for regenerative medicine in the spinal cord. Biomaterials 34:4945-4955.

Watson NV, Freeman LM, Breedlove SM (2001) Neuronal size in the spinal nucleus of the bulbocavernosus: direct modulation by androgen in rats with mosaic androgen insensitivity. J Neurosci 21:1062-1066.

Whitlock EL, Tuffaha SH, Luciano JP, Yan Y, Hunter DA, Magill CK, Moore AM, Tong AY, Mackinnon SE, Borschel GH (2009) Processed allografts and type I collagen conduits for repair of peripheral nerve gaps. Muscle Nerve 39:787-799.

Zele T, Sketelj J, Bajrovic FF (2010) Efficacy of fluorescent tracers in retrograde labeling of cutaneous afferent neurons in the rat. J Neurosci Methods 191:208-214.

Zhan X, Gao M, Jiang Y, Zhang W, Wong WM, Yuan Q, Su H, Kang X, Dai X, Zhang W, Guo J, Wu W (2013) Nanofiber scaffolds facilitate functional regeneration of peripheral nerve injury. Nanomedicine 9:305-315.

Zhang S (2008) Designer self-assembling Peptide nanofiber scaffolds for study of 3-d cell biology and beyond. Adv Cancer Res 99:335-362.

Zhang S, Gelain F, Zhao X (2005) Designer self-assembling peptide nanofiber scaffolds for 3D tissue cell cultures. Semin Cancer Biol 15:413-420.

Zhang S, Holmes T, Lockshin C, Rich A (1993) Spontaneous assembly of a self-complementary oligopeptide to form a stable macroscopic membrane. Proc Natl Acad Sci U S A 90:3334-3338.

Zochodne DW (2012) The challenges and beauty of peripheral nerve regrowth. J Peripher Nerv Syst 17:1-18.

Copyedited by Patel B, Robens J, Li CH, Song LP, Zhao M